

pubs.acs.org/cm Article

An Air-Stable and Exfoliable Ferromagnetic Two-Dimensional Perovskite, (Phenethylammonium)₂CrCl₄

Rachel T. Smith, Kelly M. Walsh, Qianni Jiang, Jiun-Haw Chu, and Daniel R. Gamelin*



Cite This: https://doi.org/10.1021/acs.chemmater.3c02824



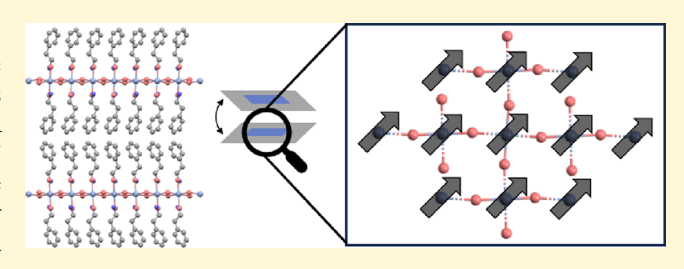
ACCESS I

III Metrics & More

Article Recommendations

s Supporting Information

ABSTRACT: Synthesis and structural characterization of the 2D hybrid-perovskite ferromagnet (PEA)₂CrCl₄ are reported (PEA = phenethylammonium). Single-crystal X-ray diffraction shows isolated inorganic sheets separated by bilayers of the bulky PEA cation. The inorganic sheets consist of networked $[\text{CrCl}_6]^{4-}$ octahedra with ordered in-plane Jahn–Teller distortions. The PEA cations impart air stability to these otherwise highly hygroscopic and oxidatively unstable compounds. $(\text{PEA})_2\text{CrCl}_4$ is ferromagnetically ordered with $T_{\text{C}}=44\,\text{K}$ and shows rich



temperature-dependent absorption in the visible region that reflects coupling of Cr^{2+} optical spin-flip transitions to 2D magnons. The van der Waals lattice structure has allowed mechanical exfoliation of monolayers with micrometer lateral dimensions, and air stability is largely retained. These attributes make $(PEA)_2CrCl_4$ an attractive platform for development of 2D perovskite chemistry that links structure, magnetism, and magneto-optics, including at the monolayer limit.

■ INTRODUCTION

Recent advances in hybrid inorganic/organic metal-halide perovskites have revealed exciting opportunities for the development of new optoelectronic materials, stimulating an explosion of research into the synthesis, structure/function relationships, and applications of these materials. 1-5 Most of this perovskite renaissance has focused on semiconducting perovskites of Pb2+ and Sn2+, driven in large part by the chemical tunability of their physical properties and the high efficiencies of lead-iodide-based (e.g., CH3NH3PbI3, or MAPbI₃) photovoltaics. 1,3,4,6,7 An intriguing family of leadfree layered metal-halide perovskites is the chromium-based compounds, A_2CrX_4 , where $A = RNH_3^+$ (e.g., $MeNH_3^+$, $EtNH_3^+$, $BzNH_3^+$) and $X = Cl^-$, Br^{-8-10} These compounds and their all-inorganic analogs (A = K⁺, Cs⁺, Rb⁺) attracted a great deal of interest in the 1970s and 1980s after they were discovered to be a unique class of "transparent ferromagnets", 11 but they have received virtually no attention since. 12,13 Most work on hybrid A₂CrX₄ compounds was thus performed before the explosion of research into hybrid lead-based 2D perovskites, and further investigation of their chemistry and properties is warranted.

One challenge confronting these materials is their atmospheric instability. A₂CrX₄ compounds have historically been extremely hygroscopic and subject to facile Cr²⁺ oxidation in air⁹; they are much less stable than analogous hybrid lead-halide perovskites. Creation of A₂CrX₄ compositions that are more stable in ambient atmosphere will ease further investigation of their properties and applications. From observations with hybrid lead-halide perovskites, ^{13,16} we hypothesized that hybrid A₂CrX₄ compounds could be

stabilized by using larger, more hydrophobic organic cations. For example, replacing small cations like methylammonium with the larger phenethylammonium (PEA) enhances leadhalide perovskite stability in ambient conditions, $^{14-17}$ and long-chain alkylammonium-based ($C_nH_{2n+1}NH_3$)₂PbI₄ 2D perovskites ($n=14,\ 16,\ 18$) show increasing stability with increasing $n.^{18}$ Air-stable A₂CrX₄ compounds have not been demonstrated previously, presenting an opportunity to test the efficacy of this strategy in a more challenging materials system.

Here, we report the synthesis of large crystals of the new hybrid compound (PEA)₂CrCl₄, via an antisolvent vapor-diffusion method. In stark contrast with the structurally analogous methylammonium compound (MeNH₃)₂CrCl₄, these (PEA)₂CrCl₄ crystals show remarkably good stability in air over many days. Since few X-ray crystal structures of A₂CrCl₄ compounds exist, the structure of (PEA)₂CrCl₄ was determined by single-crystal diffraction. This structure shows sheets of distorted [CrCl₆]⁴⁻ octahedra spaced by PEA bilayers with a van der Waals gap between them. We further demonstrate that these crystals can be mechanically exfoliated down to single monolayers with micrometer lateral dimensions. Magnetic measurements on a bulk (PEA)₂CrCl₄ single crystal show in-plane ferromagnetic ordering with $T_{\rm C} = 44~{\rm K}$,

Received: November 3, 2023 Revised: January 12, 2024 Accepted: January 16, 2024



and electronic absorption measurements at zero field allow the spontaneous 2D magnetic ordering to be monitored via evolution of Cr^{2+} spin-flip excitations. These findings highlight $(PEA)_2CrCl_4$ as an attractive candidate for studies of A_2CrX_4 magnetism and magneto-optics from the bulk to the monolayer limit, and they pave the way for its use as a model system for further experimentation with magnetic hybrid perovskites.

EXPERIMENTAL SECTION

Synthesis. (Phenethylammonium) $_2$ CrCl $_4$ ((PEA) $_2$ CrCl $_4$) crystals were grown in an inert atmosphere by dissolving CrCl $_2$ powder (1.14 mmol) and PEA-Cl (2.39 mmol) in 50:50 methanol:ethanol (20 mL) through vigorous shaking, and placing this solution in a larger container containing diethyl ether (\sim 50 mL). Slow vapor diffusion of the ether into the alcohol solution at room temperature yields large (>1 cm 2), thin, pale green, faceted crystals over \sim 18 h. Individual crystals were isolated by removing them from the mother liquor and allowing them to dry under an inert atmosphere. (Methylammonium) $_2$ CrCl $_4$ ((MeNH $_3$) $_2$ CrCl $_4$) crystals were grown by the same method using CH $_3$ NH $_3$ Cl in place of PEA-Cl.

Physical Measurements. Single-crystal X-ray diffraction data were collected at 100 K on a Bruker APEX II single-crystal diffractometer using Mo-radiation and a Miracol X-ray optical collimator. A crystal measuring 0.50 × 0.25 × 0.05 mm³ was mounted on a loop with oil. The crystal-to-detector distance was 47 mm and the exposure time was 20 s per frame for all sets. The scan width was 0.75°. The data were integrated and scaled using SAINT (version 7.34A) and SADABS (version 2007/4) within the APEX2 (version 2.1-4) software package by Bruker. Additional X-ray diffraction data were measured on single crystals using a Bruker D8 Discover powder diffractometer with a high-efficiency IµS microfocus X-ray source for Cu K α radiation operating at 50,000 mW (50 kV, 1 mA). Optical microscope images were collected using a Cannon EOS 7000 camera equipped with an Olympus optical objective (LMPlanFL N, 5x/0.15/0/FN26.5; LMPlanFL N, 20x/0.40/0/FN26.5; SLMPlan N, 50x/0.35/0/FN26.5) housed in the UW MEM-C shared facilities. Height analysis of exfoliated flakes was performed by using a Bruker Dimension Edge atomic force microscope (MEM-C Shared Facilities) operating in contact mode. Variable-temperature electronic absorption spectra were collected on a single crystal cooled in a helium flow cryostat using an Aligent Cary 5000 spectrometer. Magnetic measurements were collected on a single crystal using a Quantum Design physical property measurement system (PPMS-14T) vibrating sample magnetometer.

RESULTS AND DISCUSSION

Synthesis and Structural Characterization. Figure 1 summarizes the synthesis and basic characterization of the (PEA)₂CrCl₄ crystals reported here. Growth of A₂CrX₄-type crystals by antisolvent vapor diffusion has not been reported previously. Figure 1a describes the chemical reaction involved. Figure 1b shows a typical (PEA)₂CrCl₄ crystal obtained from this synthesis. The crystal has lateral dimensions of ~ 6 cm², thickness of <1 mm, and is nearly transparent in the visible region. Figure 1c shows an optical image of the crystal under a microscope, taken with 100× magnification. Step edges with well-defined faceting are observed on the crystal surface. Figure 1d shows X-ray diffraction data collected for an oriented (PEA)₂CrCl₄ crystal using a powder diffractometer. Select peaks are indexed according to the single-crystal X-ray structure (vide infra). The peaks in Figure 1d primarily correspond to (00l) reflections, highlighting the crystal's orientation and layer stacking along the *l* direction.

Most structural information for A₂CrCl₄ compounds has come from neutron-scattering measurements, ^{19–21} and single-

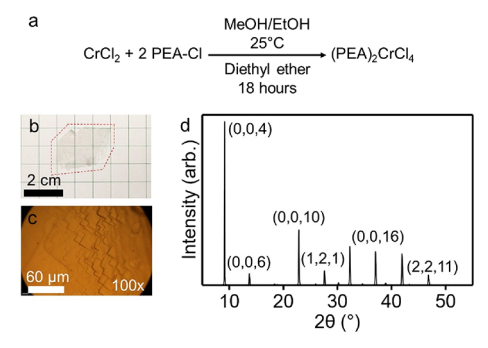


Figure 1. (a) (PEA)₂CrCl₄ crystals are formed by the vapor diffusion of diethyl ether (antisolvent) into an alcohol solution of Cr^{2+} and PEA precursors at room temperature. (b) Photograph of a (PEA)₂CrCl₄ crystal, showing distinct faceting. A dashed red line outlines the crystal as a guide for the eye. The scale bar is 2 cm. (c) Optical microscope image of a (PEA)₂CrCl₄ crystal showing multiple step edges. The scale bar is 60 μ m. (d) X-ray diffraction pattern of an oriented (PEA)₂CrCl₄ crystal collected on a powder diffractometer, with select peaks indexed.

crystal X-ray structures have only been reported for a few compounds. Because (PEA)₂CrCl₄ has not been synthesized previously, its structure was determined by single-crystal X-ray diffraction. Figure 2a summarizes the 100

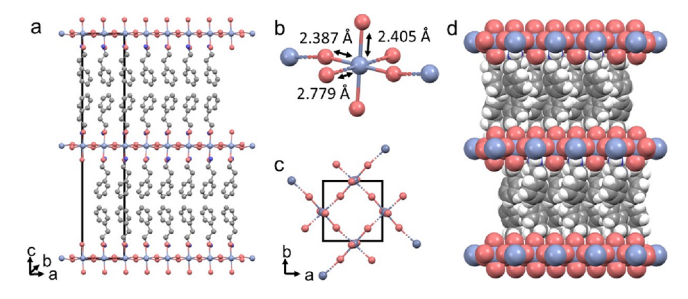


Figure 2. Single-crystal X-ray structure of $(PEA)_2CrCl_4$ collected at 100 K. (a) Edge view of the $(PEA)_2CrCl_4$ structure, illustrating 2D sheets of interconnected $[CrCl_6]^{4-}$ octahedra stacked with PEA spacers. The black lines indicate the unit cell. (b) Individual $[CrCl_6]^{4-}$ octahedron and its Cr-Cl bond lengths. The dashed bonds highlight the in-plane tetragonal elongation. (c) Top-down view of the middle 2D inorganic layer in the unit cell of panel (a), showing antiferrodistortive ordering of the Cr^{2+} Jahn-Teller elongation axes (dashed bonds). (d) Space-filling representation of the edge view of $(PEA)_2CrCl_4$ shown in panel (a).

K structure. Consistent with other hybrid A_2CrX_4 compounds, $(PEA)_2CrCl_4$ adopts the K_2NiF_4 structure type and has orthorhombic symmetry, forming in the 2D (Ruddlesden–Popper) perovskite phase with extended sheets of six-coordinate Cr^{2+} cations bridged by chloride anions. These inorganic sheets are separated by two layers of organic A-site PEA cations with a van der Waals gap between them. The interlayer separation is 1.92 nm, which is the second largest known for any A_2CrX_4 compound.

Each Cr^{2+} ion shows a large tetragonal elongation of its first coordination sphere (Figure 2b), with two Cr-Cl bonds ~0.4 Å longer than the other four. The elongation axes lie in the *ab* plane but order antiferrodistortively such that neighboring Cr^{2+} elongation axes are orthogonal to one another (Figure 2c). This cooperative Jahn-Teller distortion is a signature of the A_2CrCl_4 family of compounds. ²⁵ The elongated bond lengths of ~2.8 Å and the Cr-Cl-Cr angle of 166.3° are comparable

to those of other hybrid A_2CrX_4 compounds (see Table S3).⁸ (PEA)₂CrCl₄ also shows some octahedral tilting ($\theta_a = +5.98^{\circ}$ and $\theta_b = \pm 5.04^{\circ}$, where θ_i refers to the tilt angle toward crystallographic axis *i*, see Figure S3), as is common for many halide perovskites.^{26–29} Figure 2d shows a space filling representation of the same edge as that shown in Figure 2a.

Air Stability. (PEA)₂CrCl₄ is found to be remarkably stable in an ambient environment. To illustrate this observation, the known compound (MeNH₃)₂CrCl₄ was also prepared by the same synthesis method. Figure 3a compares two photographs

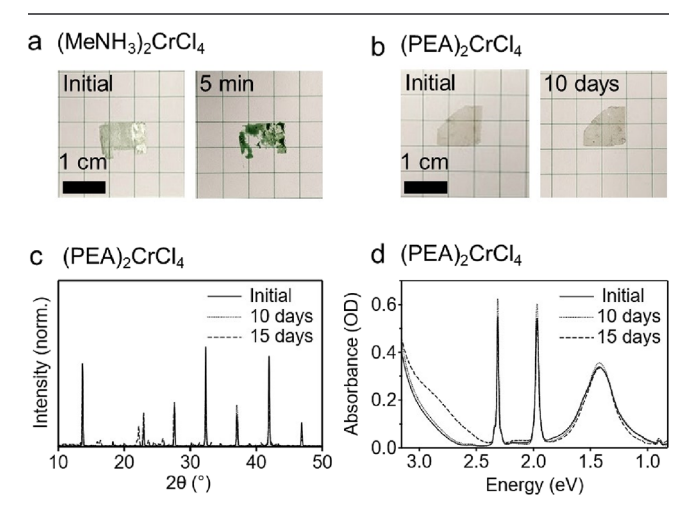


Figure 3. Air stability of the $(PEA)_2CrCl_4$ crystals. (a) Photographs of a crystal of $(MeNH_3)_2CrCl_4$ taken after initial air exposure (left) and after 5 min in air (right) showing rapid decomposition. Scale bar = 1 cm. (b) Photographs showing a similar crystal of $(PEA)_2CrCl_4$ taken after initial air exposure (left) and after 10 days in air (right), showing retention of the crystal's integrity. Scale bar = 1 cm. (c) XRD data for a $(PEA)_2CrCl_4$ crystal stored in air were collected upon initial exposure, after 10 days in air, and after 15 days in air. The initial and 10 day data are essentially indistinguishable. Peaks from a new decomposition phase become evident in the 15 day data, but the original phase is still dominant. (d) Room-temperature absorption spectra of a $(PEA)_2CrCl_4$ crystal stored in air, collected upon initial exposure, after 10 days in air, and after 15 days in air. The initial and 10 day data are again essentially indistinguishable. After 15 days in air, a broad decomposition band centered at ~2.9 eV is evident.

of the same individual (MeNH₃)₂CrCl₄ crystal: the first taken when the crystal was initially exposed to air and the second after 5 min in air. As prepared, the crystal is transparent and essentially colorless, just like that of (PEA)₂CrCl₄ (Figure 1b). After only 5 min in air, however, the (MeNH₃)₂CrCl₄ crystal completely decomposed, showing large areas that have been etched and other areas that are discolored by oxidation. In contrast, (PEA)₂CrCl₄ crystals show no detectable decomposition on the same time scale. Figure 3b compares two photographs of (PEA)₂CrCl₄ after initial exposure to air and after 10 full days in air. Even with this long exposure, the crystal's morphology remains unchanged. Figure 3c shows powder X-ray diffraction data collected on a similar (PEA)₂CrCl₄ crystal over the course of 15 days in air, normalized to the peak at $2\theta \approx 14^{\circ}$. After 10 days, the data show no significant change, and only after 15 days is diffraction from a decomposition phase evident. The original phase is still dominant. Similarly, absorption spectroscopy (Figure 3d) shows superimposable spectra for the first ~10 days, and only after ~10-15 days is a new broad band at ~2.8 eV

evident that reflects the very slow oxidation. This increased air stability could be due to the greater hydrophobicity of PEA. Notably, close packing of PEA in the ordered structure fills space effectively (Figure 2d, see also Figure S4), which helps protect chromium from the surrounding atmosphere.

Exfoliation. By changing the size of the R group on the alkylammonium cations, seminal experiments performed decades ago demonstrated that the ferromagnetism of A₂CrX₄ compounds is not significantly dependent on interlayer spacing. 9,25 From these results, it was concluded that the A2CrX4 compounds are two-dimensional easy-plane ionic ferromagnets, although the monolayer was never isolated. More recently, A₂CrX₄ compounds have also been predicted to be good candidates for mechanical exfoliation, ¹² but they have not yet been studied in this way. To test the feasibility of mechanical exfoliation, we attempted to exfoliate (PEA)₂CrCl₄ single crystals using the Scotch-tape method, transferring the resulting materials onto SiO₂ wafers under gentle heating. Figure 4a shows a large-area optical microscope image of a representative exfoliation. Many flakes with lateral dimensions of several micrometers are observed. The white arrow indicates a particularly thin flake. Figure 4b shows an AFM image collected in this area, which reveals a single monolayer of

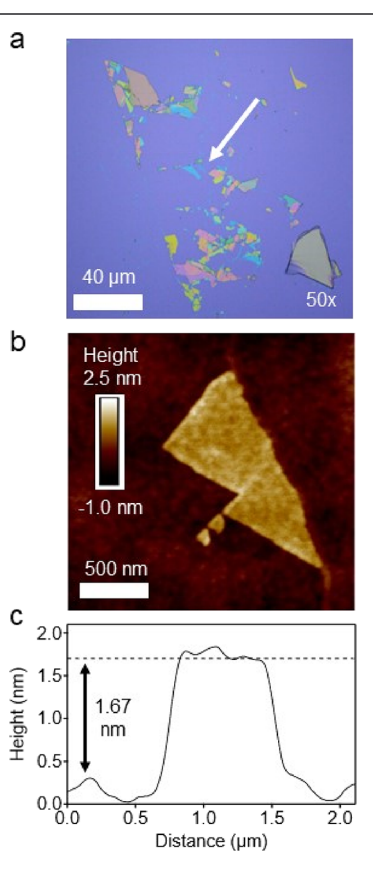


Figure 4. (a) Large-area optical image of a mechanically exfoliated (PEA)₂CrCl₄ crystal. The white arrow indicates the region where the AFM data of Figure 4b,c were collected. Scale bar: 40 μ m. (b) AFM image of the region from Figure 4a indicated by the white arrow (2.0 \times 2.0 μ m area). Scale bar: 500 nm. (c) AFM height plot for the flake shown in Figure 4b, indicating a height of ~1.67 nm, consistent with a single (PEA)₂CrCl₄ monolayer. Averaging over many AFM measurements of step heights in several other flakes gives an average monolayer height of 2.0 \pm 0.1 nm (Figure S5).

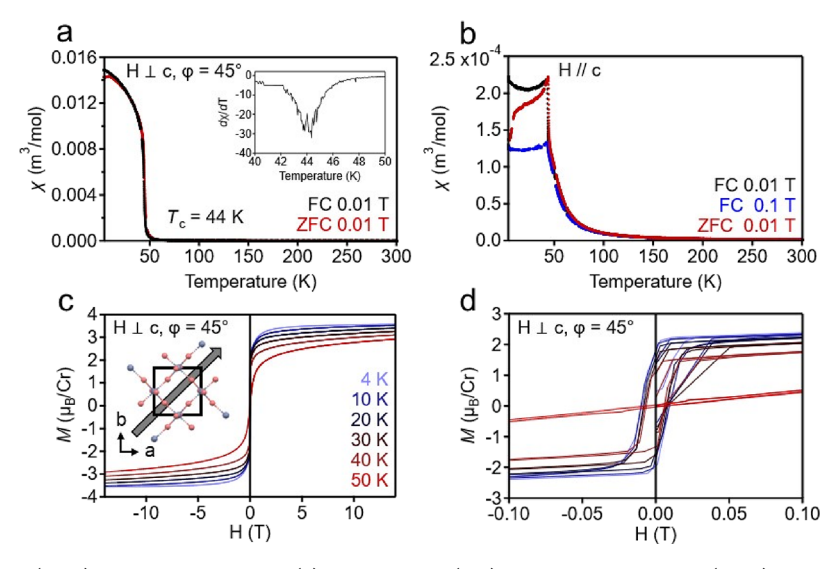


Figure 5. Magnetic data for a (PEA)₂CrCl₄ single crystal. (a) Field-cooled (FC) and zero-field-cooled (ZFC) susceptibility, measured with H = 0.01 T applied in the ab plane ($H \perp c$), bisecting the angle defined by the a and b axes ($\varphi = 45^{\circ}$). The inset shows the derivative of the FC data, yielding an ordering temperature of $T_C = 44$ K. (b) FC and ZFC susceptibility data were collected with an applied magnetic field oriented perpendicular to the crystallographic ab plane and parallel to the c axis (H//c). (c) Field-sweep magnetization data were measured from -14 to +14 T at different temperatures. The inset illustrates the in-plane magnetic-field ($H \perp c$, $\varphi = 45^{\circ}$) orientation, coinciding with a magnetic easy axis. (d) An expanded view of the data from Figure 5c, showing magnetic hysteresis at low temperatures.

(PEA)₂CrCl₄, confirmed by the height-scan data shown in Figure 4c. The thickness of this flake was determined to be 1.67 nm. The average monolayer thickness found by measuring the step heights of several flakes was determined to be 2.0 \pm 0.1 nm (Figure S5). This thickness agrees well with the monolayer thickness expected from single-crystal X-ray diffraction (~1.9 nm interlayer spacing). These data thus represent the first exfoliation of any A₂CrX₄ compound, demonstrating the ability to isolate even an individual monolayer. Importantly, AFM data for exfoliated samples (Figure S6) show no detectable change after up to 3 days in air, indicating that the protection provided by PEA against atmospheric degradation is retained, even in such thin crystals. These results demonstrate that (PEA)₂CrCl₄ is well suited to serve as a practical model system for the physical investigation of exfoliated A₂CrCl₄ compounds.

Ferromagnetism. The magnetic properties of a (PEA)₂CrCl₄ single crystal were examined using vibrating sample magnetometry and the results are summarized in Figure 5. Figure 5a plots field-cooled (FC) and zero-fieldcooled (ZFC) molar susceptibility (χ) vs temperature for a single crystal with a 0.01 T magnetic field oriented in the crystallographic ab plane $(H \perp c)$, bisecting the angle defined by the a and b axes ($\varphi = 45^{\circ}$). The data show a rapid increase in χ below ~50 K. The inset to Figure 5a plots the derivative of the FC data vs temperature, from which a value of T_C = 44 K is determined. Magnetic measurements with the field oriented perpendicular to the ab plane $(H \parallel c)$ show a similar temperature dependence but much smaller χ (Figure 5b), and those with the magnetic field oriented along either a or b ($H \perp$ $c_1 \varphi = 0^\circ$ or 90°) also reduced χ relative to $\varphi = 45^\circ$ (Figure S7). These data indicate in-plane magnetic ordering with easy axes bisecting the crystallographic a and b axes, as illustrated in the inset of Figure 5c.

Figure 5c plots magnetic-field-sweep data for the same sample, collected from -14 to +14 T ($H \perp c$ and $\varphi = 45^{\circ}$) at several temperatures. At 4 K, M saturates at 3.55 $\mu_{\rm B}/{\rm Cr}$, consistent with the ferromagnetic alignment of ${\rm Cr}^{2^+}$ spins.

Increasing the temperature slowly decreases the magnetization at a given field, similar to that in Figure 5a. Figure 5d shows the low-field region of Figure 5c on an expanded scale. A magnetic hysteresis is observed at 4 K, characterized by a coercivity of \sim 12.5 mT and remnant magnetization of \sim 2 $\mu_{\rm B}/$ Cr. Both values decrease as the temperature is raised, and at 50 K, there is no longer any evident hysteresis (Figure S7). We note that the 100 K X-ray diffraction data in Figure 2 indicate antiferrodistortive ordering well above the magnetic ordering temperature T_C consistent with a Jahn-Teller energy much greater than the inter-ion magnetic-exchange energy. 30 This cooperative Jahn-Teller distortion and its associated orbital ordering presents near-linear superexchange pathways between neighboring Cr^{2+} ions that connect the half-filled z^2 orbital (molecular coordinate frame) on one site to the empty x^2-y^2 orbital on its neighbor, yielding ferromagnetic Cr-Cr coupling and ultimately long-range in-plane ferromagnetism within the inorganic sheets.9 The antiferrodistortive ordering also orients the easy axis along $\varphi = 45^{\circ}$.

High-temperature susceptibility data for A_2CrCl_4 compounds have previously been analyzed using the series expansion given in eq 1^{20} for a Heisenberg quadratic-layer magnet with a Hamiltonian of $H = -JS_i \cdot S_j$, to estimate the nearest-neighbor magnetic-exchange constant, J.

$$\frac{Ng^2 \mu_B^2}{\chi} = \frac{1}{2}kT + J(-4 + 9x - 9.072x^2 + 55.728x^3 - 160.704x^4 + 116.640x^5)$$
 (1)

Here, $x = \frac{J}{kT}$, N is Avogadro's number, g is the Landé factor, $\mu_{\rm B}$ is the Bohr magneton, k is the Boltzmann constant, and S = 2 for high-spin d^4 Cr²⁺. After correcting for diamagnetic contributions, the susceptibility data from 70–155 K were fit to eq 1 (Figure S8), giving a value of $J = +0.87 \pm 0.01$ meV (+7.0 \pm 0.1 cm⁻¹) that is comparable to J values of other A₂CrCl₄ compounds (see Table S3 for compilation of literature results). Similarly, $T_{\rm C}$ in (PEA)₂CrCl₄ is comparable

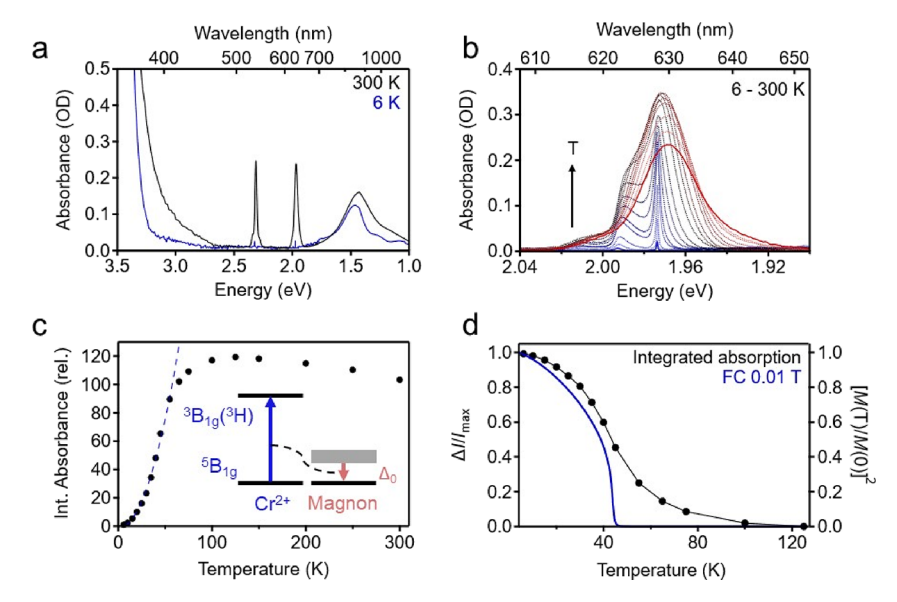


Figure 6. (a) Variable-temperature electronic absorption spectra of a (PEA)₂CrCl₄ bulk single crystal ($E \to \bot c$), collected at 6 (blue) and 300 K (black). (b) The ${}^5B_{1g} \to {}^3B_{1g}({}^3H)$ region from (a) is plotted on an expanded scale, including spectra from several intermediate temperatures. (c) Total integrated absorbance of the ${}^5B_{1g} \to {}^3B_{1g}({}^3H)$ transition from (b) plotted vs temperature. Inset: depiction of the simultaneous Cr^{2+} spin-flip excitation and annihilation of a thermally populated magnon. The dashed curve describes a T^2 temperature dependence. (d) Data from (c) (black) replotted as $\Delta I/I_{\text{max}}$, where $\Delta I = I_{\text{max}} - I(T)$. Also plotted are the field-cooled susceptibility data from Figure 5a (blue), represented here as $(M(T)/M(0))^2$.

to those of other hybrid A_2CrX_4 compounds (Table S3). Thus, although the interlayer spacing increases dramatically going from, e.g., $(MeNH_4)_2CrCl_4$ to $(PEA)_2CrCl_4$, both J and T_C are minimally affected by this structural parameter, 8,11,20,24,31,32 confirming that interlayer magnetic exchange coupling is effectively negligible. 9,25

Less obvious from these or other literature data are the microscopic magneto-structural correlations that are operative in A₂CrCl₄ compounds. One distinction is that all-inorganic A₂CrCl₄ compounds appear to show a small but significant increase in T_C relative to hybrid A₂CrCl₄ compounds (~56 K vs 46 \pm 9 K, Table S3). The all-inorganic A₂CrCl₄ compounds also have 180° Cr-Cl-Cr bond angles, whereas hybrid A₂CrCl₄ compounds (including (PEA)₂CrCl₄) generally show smaller Cr–Cl–Cr angles of $165 \pm 2^{\circ}$ (Table S3).⁸ The smaller T_C for the hybrid compounds can be attributed in part to this decrease in bond angle, which reduces orbital overlap in the dominant ferromagnetic $d_z^2 d_{x^2-y^2}$ superexchange pathway, but other factors are also important. In particular, hybrid A2CrX4 compounds show substantially greater Cr-Cl bond lengths along the tetragonal axis (2.9 \pm 0.1 Å vs 2.76 Å in Rb₂CrCl₄), which further reduces the strength of the nearestneighbor superexchange coupling. Tilting of the octahedra relative to the ab plane is also observed in the hybrid A₂CrCl₄ perovskites but not in the all-inorganic compounds (Table S3) and may reduce superexchange coupling strengths. Unfortunately, a more detailed comparison across literature samples is hindered by inconsistencies in magnetic measurement and analysis methods. Additionally, thorough structural data are lacking for most of the known A₂CrX₄ compounds. A careful systematic investigation of magnetic and structural data across multiple A2CrCl4 compounds is needed to further clarify magneto-structural correlations in this family.

Although hybrid A₂CrCl₄ compounds remain relatively underexplored, a great deal of recent research has focused on the development of analogous hybrid magnetic A₂CuCl₄ and

A₂MnCl₄ compounds, in addition to the aforementioned hybrid semiconducting A₂PbCl₄ and A₂SnCl₄ compounds. The Cu²⁺ compounds are most similar to the Cr²⁺ compounds investigated here, exhibiting an analogous in-plane antiferrodistortive ordering of local Jahn-Teller elongation axes and showing intralayer ferromagnetic ordering with weak interlayer antiferromagnetic exchange. 33-36 A₂CuCl₄ compounds have significantly lower magnetic ordering temperatures (\sim 10 K), however, and they are not transparent across the visible spectral region but instead absorb broadly due to several lowenergy spin-allowed d-d and charge-transfer transitions. As d⁹ compounds, their magnetic moments at saturation are ca. 1/4 as large as those of the A_2 CrCl₄ compounds (S = 1/2 vs S = 2). In contrast, the Mn²⁺ hybrid perovskites are not subject to Jahn-Teller distortions and thus show no antiferrodistortive ordering, and they order antiferromagnetically below ca. 40-55 K.37-39 Among the magnetic hybrid metal-halide perovskites, the A2CrCl4 compounds are thus distinctive in their relatively high magnetic ordering temperatures, their relatively large magnetic moments, and, as described below, their unique optical properties.

Magnon-Assisted Optical Spin-Flip Excitations. Figure 6a shows overview electronic absorption spectra of a bulk single crystal of (PEA)₂CrCl₄ ($\vec{E} \perp c$) collected at 6 and 300 K. The spectra are characterized by a broad charge-transfer band in the UV (\sim 3.5 eV), two sharp spin-forbidden ("spin-flip") Cr²⁺ transitions in the visible ($^5B_{1g} \rightarrow ^3B_{1g}(^3F)$) at \sim 2.3 eV and $^3B_{1g}(^3H)$ at \sim 2.0 eV), and a broad spin-allowed ligand-field transition in the near-infrared ($^5B_{1g} \rightarrow ^5B_{2g}$ at \sim 1.5 eV).⁴⁰

The most distinctive aspect of these spectra is the extremely strong temperature dependence of the two spin-flip transitions, whose integrated intensities both increase by over 2 orders of magnitude upon warming from 6 to 300 K. Figure 6b plots variable-temperature absorption data collected from 6 to 300 K in the region of the ${}^5B_{1g} \rightarrow {}^3B_{1g}({}^3H)$ spin-flip transition, and Figure 6c plots the total integrated absorbance vs temperature

for this transition. Absorption in this window is barely detectable at 6 K but increases rapidly and broadens as the temperature is raised, before turning over at ~125 K. Whereas spin-flip transitions are generally strongly forbidden for Cr²⁺, Day, Bellitto, Güdel, and others have shown that those transitions that involve the same d orbitals as participate in superexchange can couple to magnons effectively, providing a mechanism for conserving total spin angular momentum during the optical transition. 40,41 In A_2CrCl_4 compounds, these are the $^5B_{1g} \rightarrow {}^3B_{1g}(^3F)$ (~2.3 eV) and $^3B_{1g}(^3H)$ (~2.0 eV) transitions. Critically, only magnon transitions that *increase* spin angular momentum can offset the reduction in spin angular momentum of the optical excitation, and because of ferromagnetic ordering, such magnon transitions are only possible as hot bands at elevated temperatures. This constraint makes the optical spectrum strongly temperature dependent. Below $T_{\rm C}$, the spin-flip absorbance shows a T^2 temperature dependence that reflects the thermal excitation of magnons (Figure 6c, dashed). This relationship holds until very low temperatures, and it also holds well above $T_{\rm C}$.

To emphasize the latter, Figure 6d replots the absorption data from Figure 6c as $\Delta I/I_{\text{max}}$, where $\Delta I = I_{\text{max}} - I(T)$. Superimposing these data upon the infinite spin-correlation function, represented by $(M(T)/M(0))^2$ using the FC susceptibility data from Figure 5a, 42 highlights the correlation between hot exciton-magnon absorption intensity and the loss of long-range magnetic order. This comparison additionally highlights the continued growth of hot exciton-magnon absorption in the paramagnetic regime ($>T_C$), which requires intensity contributions from short-range spin correlations as well. On the low-temperature side, a deviation from simple T^2 scaling is expected to arise from the existence of an energy gap in the magnon density of states at the Brillouin zone center (Δ_0) . Fitting the low-temperature data of Figure 6c to eq 2^{41} (Figure S9) yields a value of $\Delta_0 = 0.45 \pm 0.26$ meV (3.6 \pm 2.1 cm⁻¹), consistent with the anisotropy gaps estimated for Rb₂CrCl₄ and (MeNH₃)₂CrCl₄.^{43,44} Lower-temperature absorption data are required to narrow the uncertainty in this estimate. Overall, the temperature dependence of the Cr²⁺ spin-flip excitations in (PEA)₂CrCl₄ thus provides a unique optical probe of zero-field magnetic correlations in a 2D ferromagnet.

$$I(T)\alpha T^{2} \exp\left(\frac{\Delta_{0}}{kT}\right) \tag{2}$$

CONCLUSION

In summary, the 2D hybrid-perovskite compound (PEA)₂CrCl₄ was synthesized for the first time. Single-crystal X-ray diffraction shows a structure involving 2D inorganic sheets separated by organic PEA cation layers with a van der Waals gap between the organic layers. The inorganic sheets consist of networked $[CrCl_6]^{4-}$ distorted octahedra with alternating in-plane Jahn–Teller distortion axes. These (PEA)₂CrCl₄ crystals are substantially more stable in air than other known A₂CrX₄ compounds. The Cr²⁺ spins in each 2D layer of (PEA)₂CrCl₄ are ferromagnetically ordered with T_C = 44 K, having an in-plane easy axis. Mechanical exfoliation has also been demonstrated for the first time for any A₂CrX₄ compound, and monolayers with micrometer lateral dimensions have been achieved. These attributes make (PEA)₂CrCl₄ an attractive platform for the development of 2D perovskite

chemistry that links structure, magnetism, and magneto-optics from bulk down to the monolayer limit.

ASSOCIATED CONTENT

Supporting Information

The Supporting Information is available free of charge at https://pubs.acs.org/doi/10.1021/acs.chemmater.3c02824.

Additional optical microscopy, AFM, and VSM data, data fits, structural parameters, and tabulated literature data (PDF)

Crystallographic data of (PEA)₂CrCl₄ (CIF)

AUTHOR INFORMATION

Corresponding Author

Daniel R. Gamelin — Department of Chemistry, University of Washington, Seattle, Washington 98195-1700, United States; orcid.org/0000-0003-2888-9916; Email: gamelin@uw.edu

Authors

Rachel T. Smith — Department of Chemistry, University of Washington, Seattle, Washington 98195-1700, United States; © orcid.org/0000-0002-3974-9321

Kelly M. Walsh — Department of Chemistry, University of Washington, Seattle, Washington 98195-1700, United States; Occid.org/0000-0001-5349-8816

Qianni Jiang — Department of Physics, University of Washington, Seattle, Washington 98195-1560, United States Jiun-Haw Chu — Department of Physics, University of Washington, Seattle, Washington 98195-1560, United States

Complete contact information is available at: https://pubs.acs.org/10.1021/acs.chemmater.3c02824

Notes

The authors declare no competing financial interest.

ACKNOWLEDGMENTS

This work was primarily supported by the U.S. National Science Foundation through the University of Washington Molecular Engineering Materials Center (MEM-C), a Materials Research Science and Engineering Center (DMR-2308979 to D.R.G. and J.-H.C.). Early stages of this work were performed with the support of NSF DMR-1807394 (to D.R.G.). Additional support from a Clean Energy Institute fellowship and support from an NSF Graduate Research Fellowship (1000356387) to R.T.S. are gratefully acknowledged. Single-crystal XRD measurements were collected using the UW Chemistry X-ray Diffraction Facility with the support of Dr. Werner Kaminsky and Sebastian Krajewski. Exfoliation and AFM experiments were performed using the University of Washington MEM-C Shared Facilities with the assistance of Dr. Xi Wang.

REFERENCES

- (1) Saparov, B.; Mitzi, D. B. Organic-Inorganic Perovskites: Structural Versatility for Functional Materials Design. *Chem. Rev.* **2016**, *116*, 4558–4496.
- (2) Smith, M. D.; Crace, E. J.; Jaffe, A.; Karunadasa, H. I. The Diversity of Layered Halide Perovskites. *Annu. Rev. Mater. Res.* **2018**, 48, 111–138.
- (3) Smith, M. D.; Connor, B. A.; Karunadasa, H. I. Tuning the Luminescence of Layered Halide Perovskites. *Chem. Rev.* **2019**, *119*, 3104–3139.

- (4) Kulkarni, S. A.; Mhaisalkar, S. G.; Mathews, N.; Boix, P. P. Perovskite Nanoparticles: Synthesis, Properties, and Novel Applications in Photovoltaics and LEDs. *Small Methods* **2019**, *3*, 1800231–1800246.
- (5) Blancon, J. C.; Even, J.; Stoumpos, C. C.; Kanatzidis, M. G.; Mohite, A. D. Semiconductor physics of organic-inorganic 2D halide perovskites. *Nat. Nanotechnol.* **2020**, *15*, 969–985.
- (6) Ke, W.; Stoumpos, C. C.; Kanatzidis, M. G. "Unleaded" Perovskites: Status Quo and Future Prospects of Tin-Based Perovskite Solar Cells. *Adv. Mater.* **2019**, *31*, 1803230–1803260.
- (7) Pitaro, M.; Tekelenburg, E. K.; Shao, S.; Loi, M. A. Tin Halide Perovskites: From Fundamental Properties to Solar Cells. *Adv. Mater.* **2022**, *34*, 2105844–2105890.
- (8) Day, P. Correlation of Structures and Properties of Ferromagnetic Tetrahalogenochromate(II) Salts. *J. Magn. Magn. Mater.* **1986**, 54–57, 1442–1446.
- (9) Bellitto, C.; Day, P. Organic-intercalated Halogenochromates-(II): Low-dimensional Magnets. *J. Mater. Chem.* **1992**, *2*, 265–271.
- (10) Bellitto, C.; Bauer, E. M.; Righini, G. Organic-inorganic hybrids: From magnetic perovskite metal(II) halides to multifunctional metal(II) phosphonates. *Coord. Chem. Rev.* **2015**, 289–290, 123–136.
- (11) Day, P. New Transparent Ferromagnets. Acc. Chem. Res. 1979, 12, 236–243.
- (12) Sen, D.; Jana, G.; Kaushal, N.; Mukherjee, A.; Saha-Dasgupta, T. Intrinsic ferromagnetism in atomically thin two-dimensional organic-inorganic van der Waals crystals. *Phys. Rev. B* **2020**, *102*, 054411–054416.
- (13) Ai, Y.; Sun, R.; Liao, W.; Song, X.; Tang, Y.; Wang, B.; Wang, Z.; Gao, S.; Xiong, R. Unprecedented Ferroelectricity and Ferromagnetism in a Cr²⁺-Based Two-Dimensional Hybrid Perovskite. *Angew. Chem., Int. Ed.* **2022**, *61*, No. e202206034.
- (14) Berhe, T. A.; Su, W.; Chen, C.; Pan, C.; Cheng, J.; Chen, H.; Tsai, M.; Chen, L.; Dubale, A. A.; Hwang, B. Organometal halide perovskite solar cells: degredation and stability. *Energy Environ. Sci.* **2016**, *9*, 323–357.
- (15) Saidaminov, M. I.; Mohammed, O.; Bakr, O. M. Low-Dimensional-Networked Metal Halide Perovskites: The Next Big Thing. ACS Energy Lett. 2017, 2, 889–896.
- (16) Seitz, M.; Magdaleno, A. J.; Alcázar-Cano, N.; Meléndez, M.; Lubbers, T. J.; Walraven, S. W.; Pakdel, S.; Prada, E.; Delgado-Buscalioni, R.; Prins, F. Exciton diffusion in two-dimensional metal-halide perovskites. *Nat. Commun.* **2020**, *11*, 1–8.
- (17) Leung, T. L.; Ahmad, I.; Syed, A. A.; Ng, A. M. C.; Popović, J.; Djurišić, A. B. Stability of 2D and quasi-2D perovskite materials and devices. *Commun. Mater.* **2022**, *3*, 1–10.
- (18) Kore, B. P.; Gardner, J. M. Water-resistant 2D lead(II) iodide perovskites: correlation between optical properties and phase transitions. *Mater. Adv.* **2020**, *1*, 2395–2400.
- (19) Hutchings, M. T.; Gregson, A. K.; Day, P.; Leech, D. H. Neutron Diffraction Study of the Crystal and Magnetic Structure of the Ionic Ferromagnet Cs₂CrCl₄. *Solid State Commun.* **1974**, *15*, 313–316.
- (20) Bellitto, C.; Day, P. Magnetic Susceptibility and Optical Spectra of the Organic-intercalated Two-dimensional Ferromagnets Bis-(monomethylammonium)- and Bis(monoethylammonium) Tetra-chlorochromate (II). J. C. S. Chem. Comm. 1978, 1207–1210.
- (21) Janke, E.; Hutchings, M. T.; Day, P.; Walker, P. J. Neutron diffraction study of the crystal and magnetic structure of Rb_2CrCl_4 : a two-dimensional ionic ferromagnet. *J. Phys. C: Solid State Phys.* **1983**, 16, 5959–5969.
- (22) Babar, M. A.; Ladd, M. F. C.; Larkworthy, L. F.; Povey, D. C.; Proctor, K. J.; Summers, L. J. The Crystal Structures of Propane-1,3-diammonium Tetrachlorochromate(II), a Sheet Ferromagnet, and Bis(dimethylammonium) Tetrachlorochromate(II), an Antiferromagnetic Compound Containing Isolated [Cr₃Cl₁₂]⁶⁻ Units. *J. C. S. Chem. Comm.* 1981, 1046–1047.
- (23) Day, P.; Gregson, A. K.; Leech, D. H. Optical Properties of Ferromagnetic K₂CrCl₄. *Phys. Rev. Lett.* **1973**, 30, 3.

- (24) Stead, M. J.; Day, P. Preparation, Characterization, and Magnetic Properties of Organic-intercalated Two-dimensional Ionic Ferromagnets $(C_nH_{2n+1}NH_3)_2CrCl_4$ (n=3, 5, or 12). *J. Chem. Soc., Dalton Trans.* 1982, 1081–1083.
- (25) Spin dynamics and absorption-band profiles for the planar twodimensional easy-plane ionic ferromagnet Rb₂CrCl₄. *Proc. R. Soc. London A* 1988, 415, 277–302, .
- (26) Woodward, P. M. Octahedral Tilting in Perovskites. I. Geometrical Considerations. Acta Cryst. 1997, BS3, 32-43.
- (27) Alaei, A.; Circelli, A.; Yuan, Y.; Yang, Y.; Lee, S. S. Polymorphism in metal halide perovskites. *Mater. Adv.* **2021**, *2*, 47–63.
- (28) McNulty, J. A.; Lightfoot, P. Structural chemistry of layered lead halide perovskites containing single octahedral layers. *IUCrJ.* **2021**, *8*, 485–513.
- (29) Bechtel, J. S.; Van der Ven, A. Octahedral tilting instabilities in inorganic halide perovskites. *Phys. Rev. Mater.* **2018**, *2*, No. 025401.
- (30) Polinger, V.Orbital Ordering Versus the Traditional Approach in the Cooperative Jahn—Teller Effect: A Comparative Study. In *The Jahn-Teller Effect: Fundamentals and Implications for Physics and Chemistry*, Köppel, H.; Y, D. R.; Barentzen, H., Ed.; Springer Berlin Heidelberg: Berlin, Heidelberg, 2009; pp 685—725.
- (31) Organic-inorganic layer compounds: physical properties and chemical reactions. *Philos. Trans. R. Soc. London A* 1985, 314, 145–158
- (32) Bellitto, C.; Day, P.; Wood, T. E. Magnetic Susceptibility and Optical Study of the Organic-intercalated Two-dimensional Ionic Ferromagnet Bis(benzylammonium) Tetrachlorochromate (II). *J. Chem. Soc., Dalton Trans.* 1986, 847–861.
- (33) Witteveen, H. T. Magnetic Measurements on Polycrystalline Samples of the Layer-Type Compounds Rb₂CuCl₄, Rb₂CuCl₃Br and Rb₂CuCl₂Br₂. *Physica* **1974**, *71*, 204–236.
- (34) Kassou, S.; Belaaraj, A. A Cu based layered multifunctional material: $(C_8H_{12}N)_2CuCl_4$ Optical and electronic properties. *Matter. Res. Express* **2018**, *5*, No. 076305.
- (35) Aguado, F.; Rodriguez, F.; Valiente, R.; Senas, A.; Goncharenko, I. Three-dimensional magnetic ordering in the Rb₂CuCl₄ layer perovskite structural correlations. *J. Phys.: Condens. Matter* **2004**, *16*, 1927–1938.
- (36) Han, C.; Bradford, A. J.; Slawin, A. M. Z.; Bode, B. E.; Fusco, E.; Lee, S. L.; Tang, C. C.; Lightfoot, P. Structural features in some layered hybrid copper chloride perovskites, ACuCl₄ or A₂CuCl₄. *Inorg. Chem.* **2021**, *60*, 11014–11024.
- (37) Rauh, H.; Erkelens, W. A. C.; Regnault, L. P.; Rossat-Mignod, J.; Kullmann, W.; Geick, R. Magnetic phase diagram of Rb₂MnCl₄, a quasi-two-dimensional uniaxial antiferromagnet. *J. Phys. C: Solid State Phys.* **1986**, *19*, 4503–4510.
- (38) Watanabe, N.; Kojima, N.; Ban, T.; Tsujikawa, I. Optical absorption spectra in the quasi-two-dimensional antiferromagnets $[NH_3(CH_2)_nNH_3]MnCl_4$ (n = 2,3,4,5): I. Experimental. *J. Phys. C: Solid State Phys.* 1988, 21, 4795–4808.
- (39) Septiany, L.; Tulip, D.; Chislov, M.; Baas, J.; Blake, G. R. Polar Structure and Two-Dimensional Heisenberg Antiferromagnetic Properties of Arylamine-Based Manganese Chloride Layered Organic-Inorganic Perovskites. *Inorg. Chem.* **2021**, *60*, 15151–15158.
- (40) Bellitto, C.; Brunner, H.; Güdel, H. Optical Spectroscopy of One- and Two-Dimensional Ionic Magnets of Cr²⁺: CsCrCl₃, (CH₃)₄NCrCl₃, (CH₃)₄NCrBr₃, CrCl₂, (C₂H₅NH₃)₂CrCI₄, and (C₂H₅NH₃)₂CrBr₄. *Inorg. Chem.* **1987**, *26*, 2347–2351.
- (41) Day, P.; Janke, E.; Wood, T. E.; Woodwark, D. Optical estimation of the zone-centre magnon gap in Rb₂CrCl₄: a two-dimensional easy-plane ionic ferromagnet. *J. Phys. C: Solid State Phys.* **1979**, *12*, L329–334.
- (42) Bramwell, S. T.; Day, P.; Hutchings, M. T.; Thorne, J. R. G.; Visser, D. Neutron Scattering and Optical Study of the Magnetic Properties of the Two-Dimensional Ionic Ferromagnets Rb₂CrCl₃Br and Rb₂CrCl₂Br₂. *Inorg. Chem.* **1986**, *25*, 417–421.

- (43) Janke, E.; Wood, T. E.; Ironside, C.; Day, P. Optical and magneto-optical study of the transparent ionic ferromagnet Rb₂CrCl₄. *J. Phys. C: Solid State Phys.* **1982**, *15*, 3809–3820.
- (44) Bellitto, C.; Wood, T. E.; Day, P. Low-Temperature Optical and Magneto-Optical Study of the Organic-Intercalated Two-Dimensional Ferromagnet (CH₃NH₃)₂CrCl₄. *Inorg. Chem.* **1985**, *24*, 558–562.